Low-Light-Level Cross-Phase Modulation with Double Slow Light Pulses

Bor-Wen Shiau, Meng-Chang Wu, Chi-Ching Lin, and Ying-Cheng Chen*
Institute of Atomic and Molecular Sciences, Academia Sinica, Taipei 10617, Taiwan
(Received 1 February 2011; published 11 May 2011)

We report on the first experimental demonstration of low-light-level cross-phase modulation (XPM) with double slow light pulses based on the double electromagnetically induced transparency (EIT) in cold cesium atoms. The double EIT is implemented with two control fields and two weak fields that drive populations prepared in the two doubly spin-polarized states. Group velocity matching can be obtained by tuning the intensity of either of the control fields. The XPM is based on the asymmetric M-type five-level system formed by the two sets of EIT. Enhancement in the XPM by group velocity matching is observed. Our work advances studies of low-light-level nonlinear optics based on double slow light pulses.

DOI: 10.1103/PhysRevLett.106.193006 PACS numbers: 32.80.Qk, 42.50.Gy

Large cross-phase modulation (XPM) between two single-photon pulses is crucial in many quantum information applications. Electromagnetically induced transparency (EIT) [1] provides an avenue for the implementation of XPM to obtain a large nonlinearity with a small loss. The four-level N-type system is a basic EIT-based XPM scheme [2] which has been demonstrated [3,4]. A modified XPM scheme based on the N-type system has been demonstrated too [5]. To achieve a significant cross-phase shift (XPS) with few-photon pulses, the tight focusing of the laser beams and a long atom-photon interaction time are two requirements. However, the group velocity mismatch between the probe and signal pulses in the N-type system limits the interaction time, resulting in an ultimate limit on the XPS of ~0.1 rad for single-photon pulses [6]. To overcome this limit, Lukin and Imamoğlu proposed to utilize matched double slow light pulses in XPM experiments with two atomic species [7]. Many other variant schemes such as the tripod [8–10], N-tripod [11,12], and M-type [11,13,14] systems have been proposed too. A recent experiment has demonstrated XPM with the tripod double EIT system using a hot cell in the steady-state regime [15]. Here, we report the first experimental realization of XPM based on double slow light pulses in cold atoms.

Our double EIT and XPM schemes are shown in Fig. 1(a). Two control fields (controls 1 and 2) drive the $|F=3\rangle \rightarrow |F'=3\rangle$ and $|F=4\rangle \rightarrow |F'=4\rangle$ σ^+ transitions of the D_2 line of the cesium atoms and optically pump the population to the $6S_{1/2}, |F=3, m_F=3\rangle$ ($|1\rangle$) and $|F=4, m_F=4\rangle$ ($|6\rangle$) states. Two weak fields (i.e., probe and signal) drive the $|F=4\rangle \rightarrow |F'=3\rangle$ σ^-– and $|F=3\rangle \rightarrow |F'=4\rangle$ σ^+ transitions of the D_2 line, respectively. Probe and control 1 (signal and control 2) form a Λ-type EIT for the states $|1\rangle$ to $|3\rangle$ ($|6\rangle$ to $|8\rangle$). The group velocities of the probe and signal pulses can be easily adjusted to the matching point by varying the intensity of either of the control fields. Compared to other schemes for obtaining group velocity matching [16], our scheme is much more flexible because there are infinite sets of matching conditions.

All laser fields also drive the Zeeman sublevels of the same hyperfine level. The five states $|1\rangle$ to $|5\rangle$ and the other five $|6\rangle$ to $|10\rangle$ form two sets of asymmetric M-type systems (denoted by M_1 and M_2) [13,14]. In the M_1 system, the probe (signal) drives the Λ section with (without) the population while in the M_2 system the roles of these two fields interchange. This M-type model is not a complete description of the system because there are more Zeeman sublevels involved. However, in the weak probe and signal limit, the XPM is dominated by the $\chi^{(3)}$. Taking the M_1 system as an example, the probe susceptibility can be expressed as $\chi_p \simeq \chi_p^{(1)} + \chi_p^{(3,\mathrm{SPM})}|E_p|^2 + \chi_p^{(3,\mathrm{XPM})}|E_s|^2$ [13,14], where $\chi_p^{(1)}$, $\chi_p^{(3,\mathrm{SPM})}$, and $\chi_p^{(3,\mathrm{XPM})}$ are the linear, self-Kerr, and cross-Kerr susceptibilities, respectively, and $E_{p(s)}$ is the electric field amplitude of the probe (signal). We keep both control fields and the probe on their resonances and thus $\chi_p^{(1)}$ is a constant. The XPM of the probe is obtained by introducing a two-photon detuning in the signal's EIT system. Since only the phase difference, with and without the presence of the signal field, is measured, the $\chi_p^{(3,\mathrm{SPM})}$ is not in consideration. The explicit form of $\chi_p^{(3,\mathrm{XPM})}$ for the M_1 and M_2 system can be referred to Ref. [14,17].

Under the assumptions of the slowly varying amplitudes and negligible absorption and dispersion, the XPS of the probe pulse can be expressed as [13,14]

$$\phi_p^{\mathrm{XPM}} = \frac{\mathrm{kl}\pi^{1/2}\hbar^2|\Omega_s^{\mathrm{peak}}|^2}{4|\mu_s|^2}\frac{\mathrm{erf}[\zeta_p]}{\zeta_p}\,\mathrm{Re}[\chi_p^{3,\mathrm{XPM}}], \quad (1)$$

with $\zeta_p = (1 - v_g^p/v_g^s)\sqrt{2l}/(v_g^p\tau_s)$, where k is the probe wave vector, l is the medium length, $v_g^{p(s)}$ is the group velocity for the probe (signal), μ_s is the transition dipole moment of the signal transition, and τ_s is the $1/e$ half duration of the signal electric field. The term $\frac{\mathrm{erf}[\zeta_p]}{\zeta_p}$ describes the degree of overlapping between the two pulses

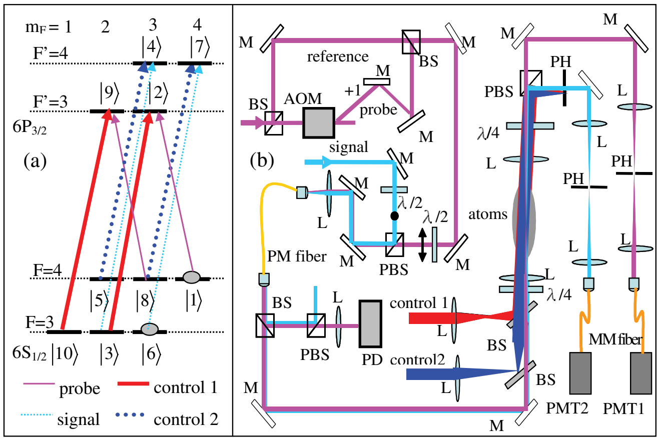

FIG. 1 (color online). (a) Relevant energy levels of ^{133}Cs atoms and laser excitations. (b) The XPM experimental setup. M, mirror; L, lens; BS, beam splitter; PBS, polarizing beam splitter; AOM, acousto-opitc modulator; $\lambda/4$, quarter-wave plate; $\lambda/2$, half-wave plate; PH, pinhole; PMT, photomultiplier tube; PM fiber, polarization-maintaining fiber; MM fiber, multimode fiber.

and it reaches a maximum value of $2/\sqrt{\pi}$ when the group velocities of the two pulses are equal. This highlights the importance of the group velocity matching.

Our experiment is based on a two-dimensional magneto-optical trap (MOT) [18] with optically dense atomic samples. The experimental setup is shown in Fig. 1(b) and is described in detail in the supplemental material [17]. Here, we briefly describe those parts related to the phase measurement. The probe beam is combined with a far-detuned reference beam to form a beat note interferometer [19]. The probe and signal beams are coupled into a polarization-maintaining fiber to ensure perfect overlapping. Before entering the MOT, parts of the probe and reference beams are detected by a photodetector (NewFocus 1801). This beat note is used to trigger an oscilloscope (Tektronix DPO4104). After passing through the MOT, the probe and reference beams are detected by a photomultiplier tube (PMT, Hamamatsu H6780-20). The beat note is averaged over 512 times and then saved for phase shift analysis. The probe pulse is divided into tens of section. Each section is fit to a sinusoidal curve to obtain the phase shift versus time. Three subsequent probe pulses separated by 50 μs and one signal pulse coincident with the last probe pulse are applied. The phase differences between the first and the second probe pulses, with typical rms values of less than 0.02 rad, serve as a check of the reliability of the measurement. The phase differences between the second and the third probe pulses are the XPSs. Whether the slope of the phase versus time for a Gaussian probe pulse in an EIT system is positive or negative indicates if its two-photon detuning is blue or red [19]. This allows us to determine the EIT resonances to 1 kHz level. We found a two-photon shift in the probe EIT resonance of within 200 kHz induced by the off-resonant excitations of the control fields. We tune the probe frequency to EIT resonance every time the control intensity is varied.

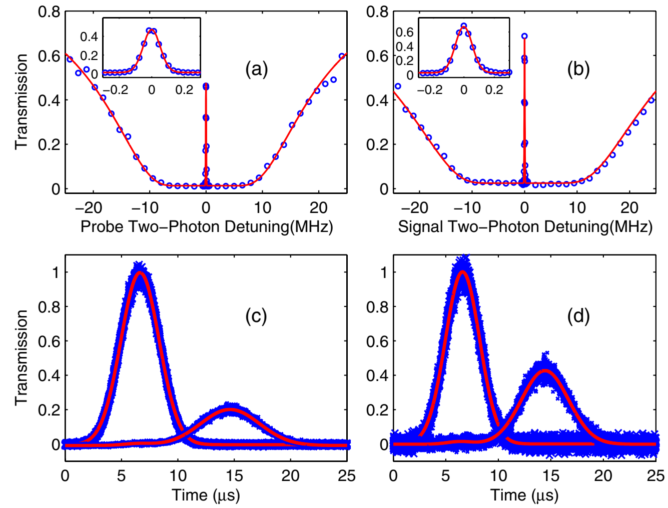

FIG. 2 (color online). (a),(b) Typical EIT spectrum for the probe and signal. The solid lines indicate the fitting curves with parameters described in the main text. The insets zoom in on the central EIT peaks. (c),(d) The slow light pulses for the probe and signal under the same parameters. The reference pulses without the presence of cold atoms are also shown. The solid lines are the Gaussian fitting curves.

The typical EIT spectra are plotted in Figs. 2(a) and 2(b). The solid lines are the fits to the EIT line shape with the fitting parameters α, Ω_c, γ, δ_c, ϵ, which are the optical depth (OD), Rabi frequency of the control, ground-state decoherence rate, control detuning, and an offset in the transmission due to a small incorrect frequency component, respectively. The values of the parameters α_p, Ω_{c1}, γ_p, α_s, Ω_{c2}, γ_s in Fig. 2 are 53, 0, 42Γ, $1.64 \times 10^{-3}\Gamma$, 87, 0.54$\Gamma$, $0.81 \times 10^{-3}\Gamma$, respectively. The FWHM linewidths for the central EIT peaks for the probe and signal are 122 and 132 kHz, respectively. The intensity FWHM durations of the input Gaussian pulses are 4 μs. Given these parameters, the slow light behaviors are shown in Figs. 2(c) and 2(d). The group delays are both 8.7 μs.

Figure 3(a) shows the group delays for the probe ($T_{D,p}$) and signal ($T_{D,s}$) versus the Ω_{c2}. The group velocity matching condition is obtained at $\Omega_{c2} = 0.51\Gamma$. The $T_{D,s}$ follows a simple relation $T_{D,s} = \alpha_s\Gamma/\Omega_{c2}^2$ if $\gamma\Gamma \ll \Omega_{c2}^2$ [1]. The solid line in Fig. 3(a) shows a plot of this relation with $\alpha_s = 80$. The $T_{D,p}$, α_p, and α_s vary a little among the Ω_{c2} as shown in Figs. 3(a) and 3(b). Figures 3(c) and 3(d) show the corresponding intensity transmission and FWHM duration (τ_{FWHM}) of the slow light pulses. In the perturbation limit, the propagation properties of the slow light pulses can be calculated by the Fourier transform method using the obtained atomic response function by solving the steady-state optical Bloch equation [20]. Considering up to the second order dispersion, one can show that after passing through a medium the intensity width of a Gaussian pulse is broadened by a factor of $\beta = \sqrt{1 + (16\ln 2\alpha_s\Gamma^2/\tau_{\mathrm{FWHM}}^2\Omega_{c2}^4)}$ and the peak intensity

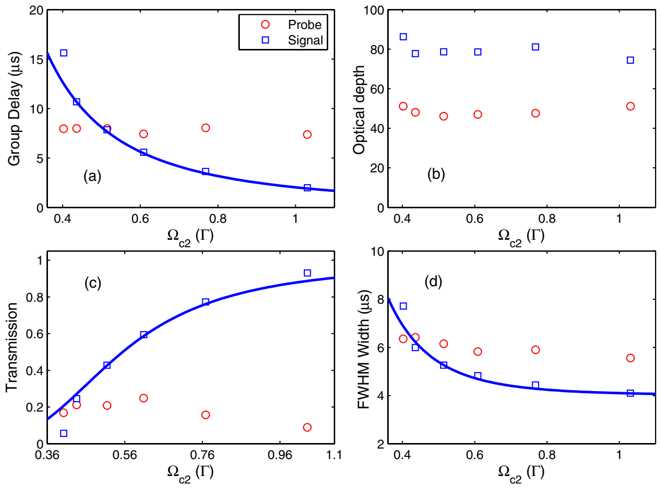

FIG. 3 (color online). (a) Group delays of the probe and signal versus the Ω_{c2}. (b) The ODs for the probe and signal versus the Ω_{c2}. (c) The intensity transmission and the FWHM duration of the slow light pulses versus the Ω_{c2}. In (a), (c), and (d) the solid lines are the theoretical curves described in the main text.

is reduced by a factor of $\exp(-\frac{\gamma\alpha_s\Gamma}{\Omega_{c2}^2})\frac{1}{\beta^2}$. The solid lines in Figs. 3(c) and 3(d) indicate the plots of these two relations with $\gamma = 0.001\Gamma$ and $\alpha_s = 80$.

We first study the steady-state XPM behavior of the M-type system. Square pulses for both the signal and probe are applied with a duration long enough such that the probe response will reach a steady-state value. Figure 4(a) shows a plot of the transmission of the probe and signal versus the detuning of the signal δ_s after being turned on for 10 μs. The signal transmission shows the characteristic EIT spectrum for a dense medium since it is dominated by the $\chi_s^{(1)}$. The probe transmission also shows an EIT-like spectrum with a much wider linewidth. However, the probe is kept at zero detuning. The transmission profile is due to the $\mathrm{Im}[\chi_p^{(3,\mathrm{XPM})}]$ introduced by the signal field. The $\mathrm{Re}[\chi_p^{(3,\mathrm{XPM})}]$ causes the XPS of the probe, as shown in Fig. 4(b). The peak power of the signal field is 50 nW.

We perform a numerical calculation of the optical Bloch equation for the ten-level system as shown in Fig. 1(a). Both the steady-state and the transient responses are calculated. The Runge-Kutta method is used for the transient calculation. The susceptibility for the transition $|i\rangle \rightarrow |j\rangle$ is related to the density matrix element ρ_{ji} by $\chi = \frac{-2n_a\mu_{ji}^2\rho_{ji}}{\hbar\epsilon_0\Omega_i}$. The intensity transmission T and the phase shift ϕ are calculated by the relations $T = \exp[\mathrm{Im}(-\chi)kl]$ and $\phi = \frac{1}{2}\mathrm{Re}(\chi)kl$. The α_s, α_p, Ω_{c1}, and Ω_{c2} are determined experimentally from the EIT spectral fittings. The decoherence rates for the six ground states are modeled by a single effective rate γ. The intensity ratio of the probe and signal is known experimentally. The excited-state decoherence rate is set to a value of $1.5\Gamma/2$, larger than $\Gamma/2$, to fit the relatively wide wings in the spectra. The decoherence in the wings is mainly due to the one-photon effect which

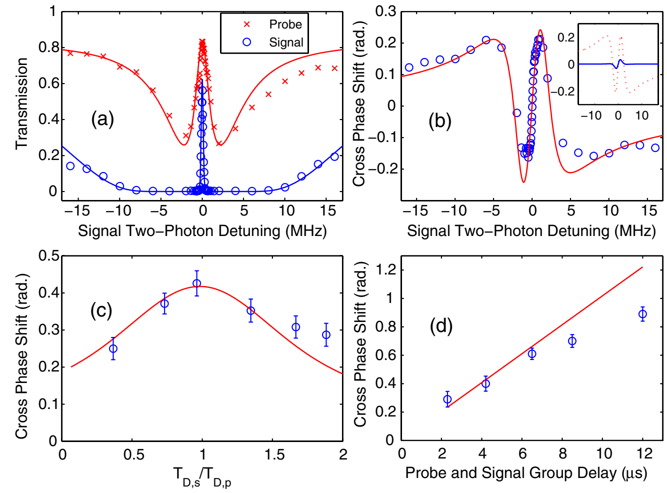

FIG. 4 (color online). (a) Transmission of the probe and signal and (b) the XPS for the probe versus the detuning of the signal. The solid lines in (a) and (b) are the theoretical curves using the ten-level transient calculation. The dotted and solid lines in the inset of (b) indicate the calculated XPS results from the $|1\rangle \rightarrow |2\rangle$ and $|8\rangle \rightarrow |9\rangle$ transition, respectively. The parameters are shown in the main text. (c) The maximum XPS for the probe versus the $r = T_{D,s}/T_{D,p}$. The solid line shows a plot of the relation (2), scaled down by a factor of 0.8, with $\Omega_s = 0.11\Gamma$. (d) The maximum XPS versus the group delays for the probe and signal, tuned to the same values. The solid line shows a plot of the relation (3) with $\Omega_s = 0.11\Gamma$.

may be contributed from finite laser linewidth and frequency jitters. In the calculation, the Ω_s is varied to fit the observed spectrum. The solid lines in Figs. 4(a) and 4(b) are the calculated spectra at 10 μs with the values for $\{\alpha_p, \alpha_s, \Omega_{c1}, \Omega_{c2}, \gamma\}$ of $\{84, 51, 1.12\Gamma, 0.76\Gamma, 0.0024\Gamma\}$. The calculation results agree well with the data when $\Omega_s = 0.11\Gamma$, with respect to the $|3\rangle \rightarrow |4\rangle$ transition. The dotted and solid lines in the inset of Fig. 4(b) show the calculated contributions of the XPS through the $|1\rangle \rightarrow |2\rangle$ and $|8\rangle \rightarrow |9\rangle$ transitions, respectively. The line shapes are the same as the $\chi_p^{(3,\mathrm{XPM})}$ for the M_1 and M_2 as calculated from perturbation theory [17]. The contribution from M_1 is larger than that from M_2 due to the higher population ratio in the state $|1\rangle$. Clear asymmetries in the XPM spectra are observed. The mechanism of this asymmetry is still unclear. We have checked that the measured XPSs are linearly dependent on the signal intensity within the saturation power of our PMT (75 nW).

Next, we studied the effect of group velocity matching on the XPM in the pulse regime. Since a pulse with a Gaussian waveform preserves its shape during the propagation and can be modeled analytically, we apply the probe and signal pulses with such a waveform. The XPS for a Gaussian probe pulse is time dependent. In the discussion below, the XPS refers to that measured at the center of the delayed probe pulse. At a fixed $T_{D,p}$ (~ 8 μs), we vary the Ω_{c2} to tune the $T_{D,s}$ and to perform the XPM measurement for various δ_s. The maximum XPS versus the group delay ratio $r = T_{D,s}/T_{D,p}$ are plotted in Fig. 4(c). The α_p and α_s are 45 and 60, respectively. The maximum XPS occurs when $r \simeq 1$. This demonstrates the effect of the group velocity matching in obtaining the large XPM. Since the contribution from M_1 is larger, and for simplicity in the analysis, we first consider the XPM from the M_1 system. From (1) and the relation for $\chi^{(3,\mathrm{XPM})}_{p,M1}$ [17], it can be shown that the maximum XPS

$$\phi^{\mathrm{XPM}}_{p,\max} = \frac{\sqrt{\pi}\alpha_p}{8} \frac{\mathrm{erf}(\zeta_p)}{\zeta_p} \frac{\Omega_s^2}{\Omega_{c1}^2}, \tag{2}$$

if $\gamma\Gamma \ll \Omega_{c1}^2$. The solid line in Fig. 4(c) shows a plot of this relation with $\alpha_p = 45$, $\Omega_{c1} = 0.50\Gamma$, $\Omega_s = 0.11\Gamma$, and a scaling factor of 0.8. Such a simplified consideration qualitatively captures the major trend in the data. However, more sophisticated analysis based on the Maxwell-Bloch equations is required to quantitatively compare the data, taking into account the nonadiabatic effect, pulse attenuation and broadening, the transverse intensity profile of the laser beams, and all XPM contributions from the ten-level system. By comparing the $r \simeq 1$ point to the extrapolated $r = 0$ point in which the signal propagates at vacuum light speed, the enhancement factor due to group velocity matching is $\sim$2. However, such a consideration overestimates the enhancement, if the contribution from M_2 is included. The XPS depends on the overlapping factor as well as on the Re$[\chi_p^{3,\mathrm{XPM}}]$. From relation (1), $\chi^{(3,\mathrm{XPM})}_{p,M1}$ and $\chi^{(3,\mathrm{XPM})}_{p,M2}$ [17], it can be shown that the maximum of the Re$[\chi^{(3,\mathrm{XPM})}_{p,M1}]$ has no dependence on the Ω_{c2} (and thus the $T_{D,s}$) but that from the M_2 does have a slight dependence on the $T_{D,s}$. With the parameters for Fig. 4(c), we estimate that $\sim$30% of the enhancement is from the variation of Re$[\chi_p^{(3,\mathrm{XPM})}]$.

We then fixed at the matching conditions and vary the group delays for both pulses together. Figure 4(d) shows the maximum XPS versus the group delay. It has a nearly linear dependence. To understand this, we consider the XPM contribution from the M_1 system only. By setting the overlapping factor to its maximum value and putting the relation $T_{D,p} = \alpha_p\Gamma/\Omega_{c1}^2$ into relation (2), we obtain a simple relation for the maximum XPS,

$$\phi^{\mathrm{XPM}}_{p,\max} = \frac{\Omega_s^2}{4\Gamma} T_{D,p}. \tag{3}$$

The solid line in Fig. 4(d) indicates a plot of this relation with $\Omega_s = 0.11\Gamma$. We emphasize that the observed nearly linear dependence on the T_D is true only with large enough ODs. Otherwise, the signal broadens and decays significantly for long group delays. The gain in the interaction time may be compensated by the loss in the interaction strength. With ODs on the order of 30, the observed XPSs are almost constant for different T_D.

The 0.89 rad XPS shown in Fig. 4(d) is the largest we have ever obtained. The additional probe loss at the maximum XPS value compared to that at zero δ_s is 37%. The obtained XPS is 1.0×10^{-6} rad per signal photon. If one could focus the beam down to the atomic absorption cross section $3\lambda^2/2\pi$, the single-photon-level XPS would be 0.015 rad. Without the double slow light scheme, the M-type XPM limit is the same as for the N-type system [21]. Considering the averaged Clebsch-Gordan coefficients for the signal transitions in our scheme, this limit is 0.046 rad per signal photon. Although we have used the double slow light scheme, the result is still a factor of 3 less than the limit without such a scheme. The reason lies in a drawback to the current scheme. A detuning on the signal's EIT system is required to induce the XPM on the probe. The large loss of the signal due to the $\chi_s^{(1)}$ degrades the performance of XPM. To implement a modified scheme with a significant $\chi_p^{3,\mathrm{XPM}}$ but with both EIT systems on their two-photon resonances will be necessary to take full advantage of the double slow light scheme. This development will be addressed in future work.

We acknowledge fruitful discussions with Ite A. Yu and Yong-Fong Chen. This work was supported by the National Science Council of Taiwan under NSC Grants No. 97-2112-M-028-MY3, No. 98-2628-M-001-003, and No. 99-2628-M-001-021.

*chenyc@pub.iams.sinica.edu.tw

[1] For a review, see, e.g., M. Fleischhauer, A. Imamoglu, and J. P. Marangos, Rev. Mod. Phys. **77**, 633 (2005).
[2] H. Schmidt and A. Imamoğlu, Opt. Lett. **21**, 1936 (1996).
[3] L. V. Hau *et al.*, Nature (London) **397**, 594 (1999).
[4] H. Kang and Y. Zhu, Phys. Rev. Lett. **91**, 093601 (2003).
[5] Y.-F. Chen *et al.*, Phys. Rev. Lett. **96**, 043603 (2006).
[6] S. E. Harris and L. V. Hau, Phys. Rev. Lett. **82**, 4611 (1999).
[7] M. D. Lukin and A. Imamoğlu, Phys. Rev. Lett. **84**, 1419 (2000).
[8] D. Petrosyan and Gershon Kurizki, Phys. Rev. A **65**, 033833 (2002).
[9] S. Rebić *et al.*, Phys. Rev. A **70**, 032317 (2004).
[10] D. Petrosyan and Y. P. Malakyan, Phys. Rev. A **70**, 023822 (2004).
[11] Z.-B. Wang, K.-P. Marzlin, and B. C. Sanders, Phys. Rev. Lett. **97**, 063901 (2006).
[12] M. A. Antón *et al.*, Opt. Commun. **281**, 6040 (2008).
[13] C. Ottaviani *et al.*, Phys. Rev. Lett. **90**, 197902 (2003).
[14] C. Ottaviani *et al.*, Eur. Phys. J. D **40**, 281 (2006).
[15] S. Li *et al.*, Phys. Rev. Lett. **101**, 073602 (2008).
[16] A. MacRae, G. Campbell, and A. I. Lvovsky, Opt. Lett. **33**, 2659 (2008).
[17] See supplemental material at http://link.aps.org/supplemental/10.1103/PhysRevLett.106.193006 for the explicit form of the $\chi_p^{(3,\mathrm{XPM})}$ for the M_1 and M_2 systems and the experimental details.
[18] Y.-W. Lin *et al.*, Opt. Express **16**, 3753 (2008).
[19] Y.-F. Chen *et al.*, Phys. Rev. A **72**, 033812 (2005).
[20] Y.-F. Chen *et al.*, Phys. Rev. A **74**, 063807 (2006).
[21] A. B. Matsko *et al.*, Opt. Lett. **28**, 96 (2003).